"Spatial and Temporal Confinement of Salt Fluxes for the Shape-Controlled Synthesis of Fe_2O_3 Nanocrystals"

Amanda K. P. Mann, Jie Fu, Christopher J. DeSantis, and Sara E. Skrabalak*

Supporting Information

Discussion of Flux Additive

The temperatures experienced by the aerosol droplets are typically much lower than that reported from the furnace on account of the short residence times of the droplets (<1 minute). Our prior experience with aerosol-assisted synthetic techniques has found that the furnace temperature of *our reactor* needs to be ~200 degrees greater than that required to induce a particular chemical or physical change indicated by thermal analysis of a precursor. On account of the stability of reactor components, 915 °C is typical upper limit for our experiments, so $Bi(NO_3)_3$ was incorporated as a flux additive to depress the melting point of the reaction media. $Bi(NO_3)_3$, is a common flux additive as the bulky size of Bi^{3+} ions precludes their intercalation into many crystal structures.

The amount of $Bi(NO_3)_3$ added was determined by trial and error and the amount reported in the manuscript is the optimized concentration which consistently yielded the highest quality product particles in terms of crystal habit. The ratio of Fe_2O_3 colloids to $Bi(NO_3)_3$ was varied with ratios of 1:1, 1:2, 1:10, and 1:0, with 1:10 being the optimal ratio.

The role of Bi ions in this synthesis is unclear at this point as it modifies the melting point of the flux but can also change the solubility of reagents and serve as a structure directing agent.

Discussion of Temperature

The syntheses reported in *Results and Discussion* were all conducted with a furnace temperature of 900 °C or 915 °C to facilitate more facile comparisons between systems. This temperature was determined by evaluating a range of temperatures (750 to 950 °C) for their ability to yield high quality samples in terms of phase purity and uniform crystal habit between particles. For several precursor formulations, lower temperatures produced high quality particles of the same shape compared to those discussed in *Results and Discussion* (e.g., $Fe_2O_3/Bi(NO_3)_3/Li_2CO_3$-$Na_2CO_3$ yielded octahedra from 750 to 900 °C and $Fe_2O_3/Bi(NO_3)_3/Na_2CO_3$ produced hexagonal plates at 875 °C). If the temperature was not adequate to facilitate dissolution of the precursor colloids, the original colloids or agglomerated colloids were obtained.

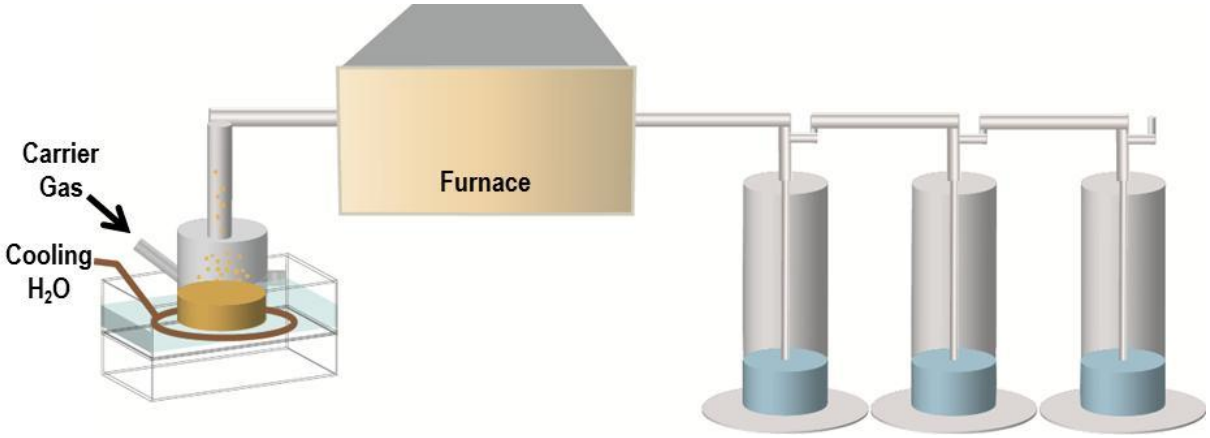

Figure S1. Schematic of experimental setup for aerosol-assisted MSS. The nebulization source consists of a Vicks V5100N Ultrasonic Humidifier base (1.7 MHz, ~5 W/cm2) filled with water as the coupling media; the base has been modified to accommodate glassware of varying size. The nebulization chamber has a gas inlet; the bottom of the nebulization cell has a 52 mm diameter opening with an O-ring groove (Chemglass: CG-138-02). A Saran wrap membrane is clamped between a Teflon base with a greased O-ring and the nebulization chamber. The nebulization chamber is then centered above the ultrasonic transducer at a distance of ~2.5 cm and filled with ~15 mL of precursor solution (room temperature). A stainless steel tube (diameter ~2.5 cm) is used with the single zone furnace (total heated region of ~30 cm, 1100 °C achievable). In all experiments, house air (210 sccm) was used to sparge the precursor solutions for 30 minutes and then as a carrier (210 sccm) once the humidifier was turned on, generating a mist. The droplet residence times were estimated to be ~5-20 seconds depending on the furnace temperature. Product is collected in a series of 3 water-filled gas washing bottles, although the quantity of product collected can be increased with the use of additional gas washing bottles. Note: while a Vicks V5100N Ultrasonic Humidifier base was used in this study, other household humidifiers can be used without changing the properties of the product, so long as the properties of the transducer remain similar. The system is also robust to small changes in dimensions.

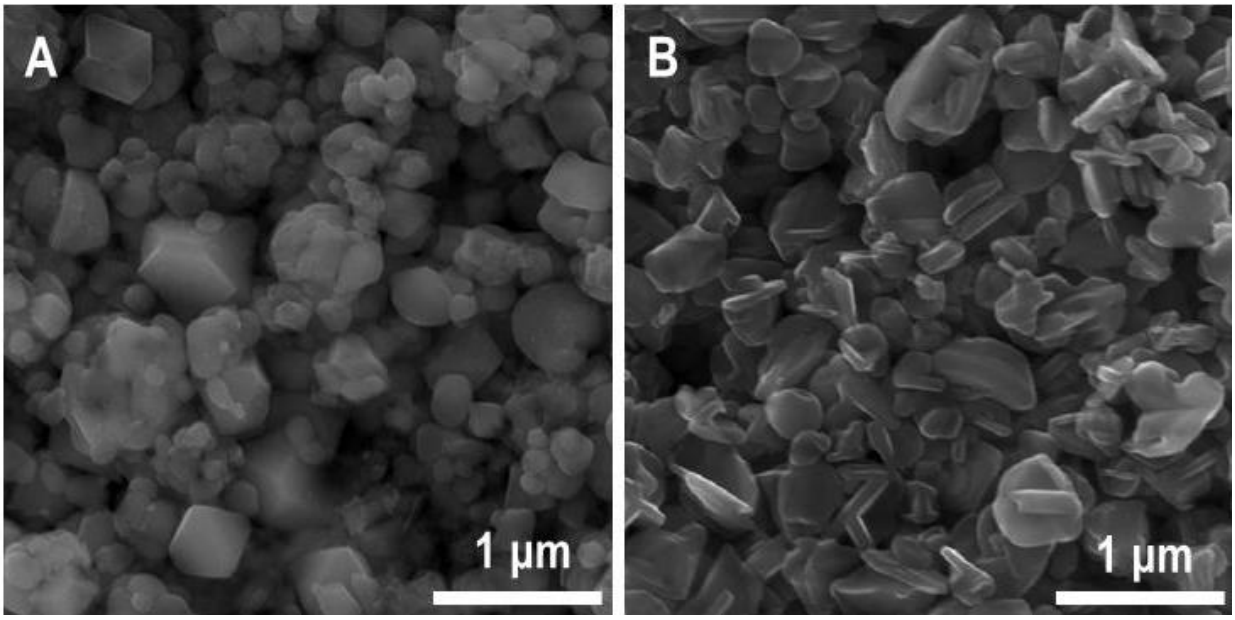

Figure S2. SEM images of the products obtained in the absence of $Bi(NO_3)_3$ but otherwise using the optimized conditions with (A) γ-Fe_2O_3 precursor colloids and Li_2CO_3 or (A) γ-Fe_2O_3 precursor colloids and K_2CO_3.

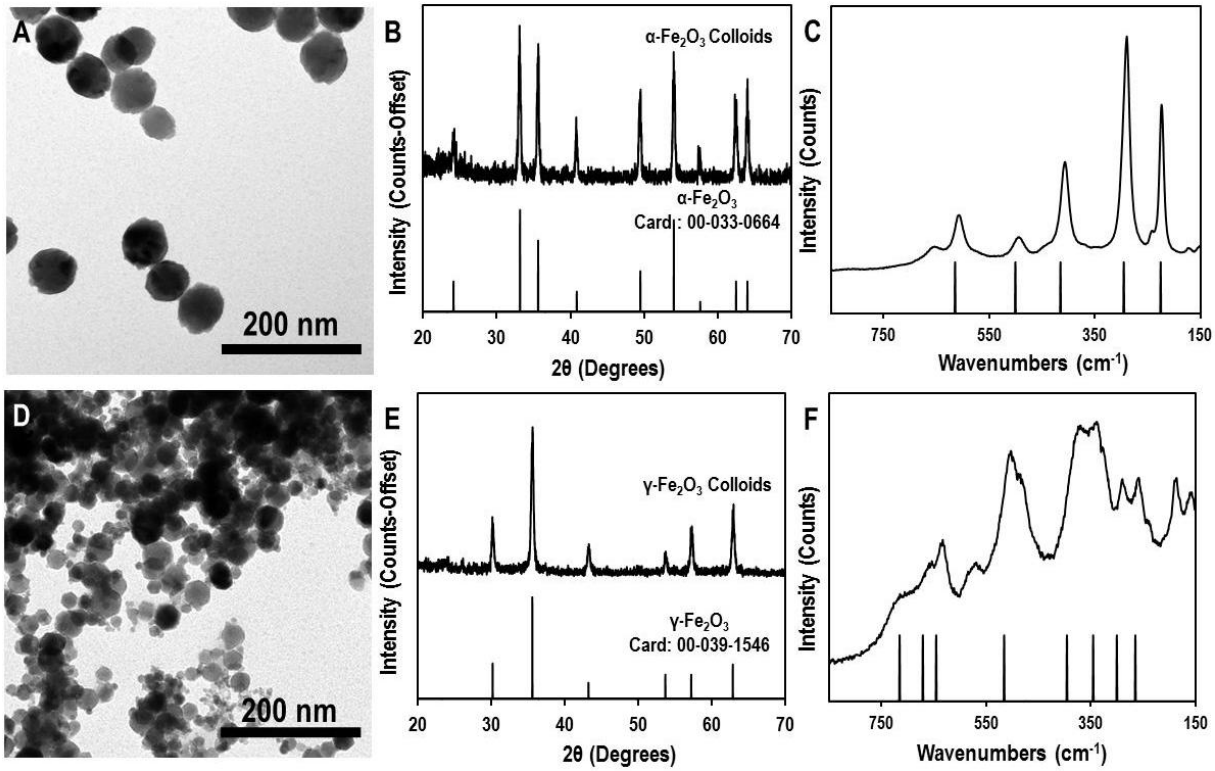

Figure S3. (A) TEM image and (B) corresponding XRD and (C) Raman spectrum of the α-Fe_2O_3 precursor colloids and (D) TEM image and (E) corresponding XRD and (F) Raman spectrum of the γ-Fe_2O_3 precursor colloids.

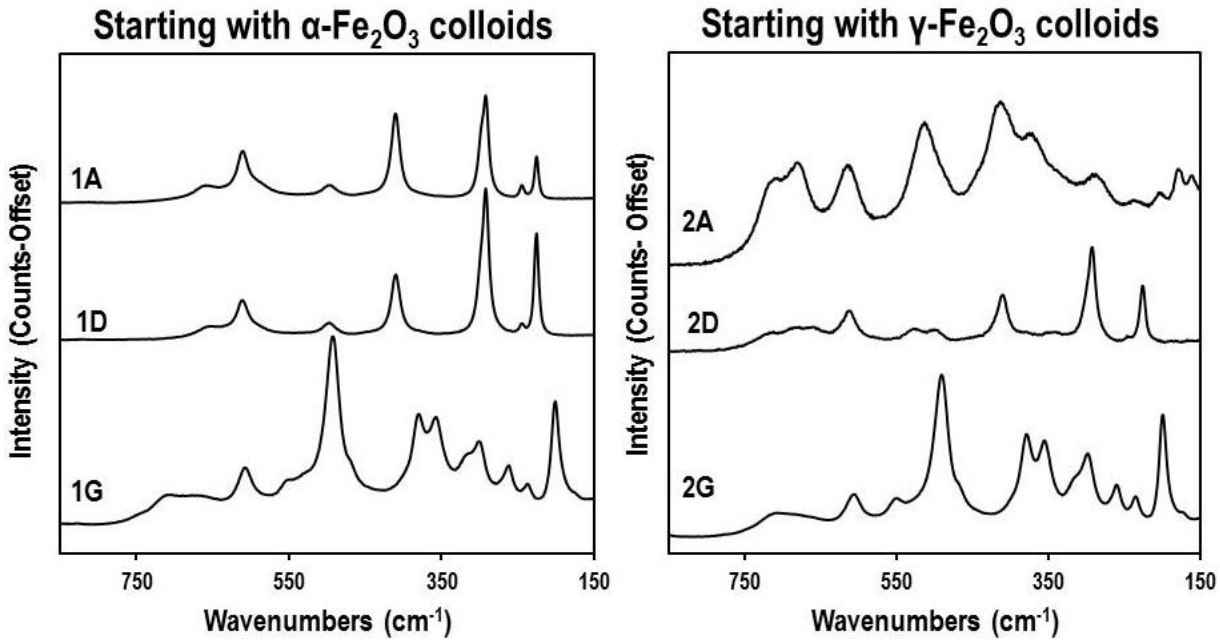

Figure S4. Raman spectra of the samples shown in Figures 1 and 2 (e.g. 1A correlates to Figure 1A, 1D correlates to Figure 1D, etc.).

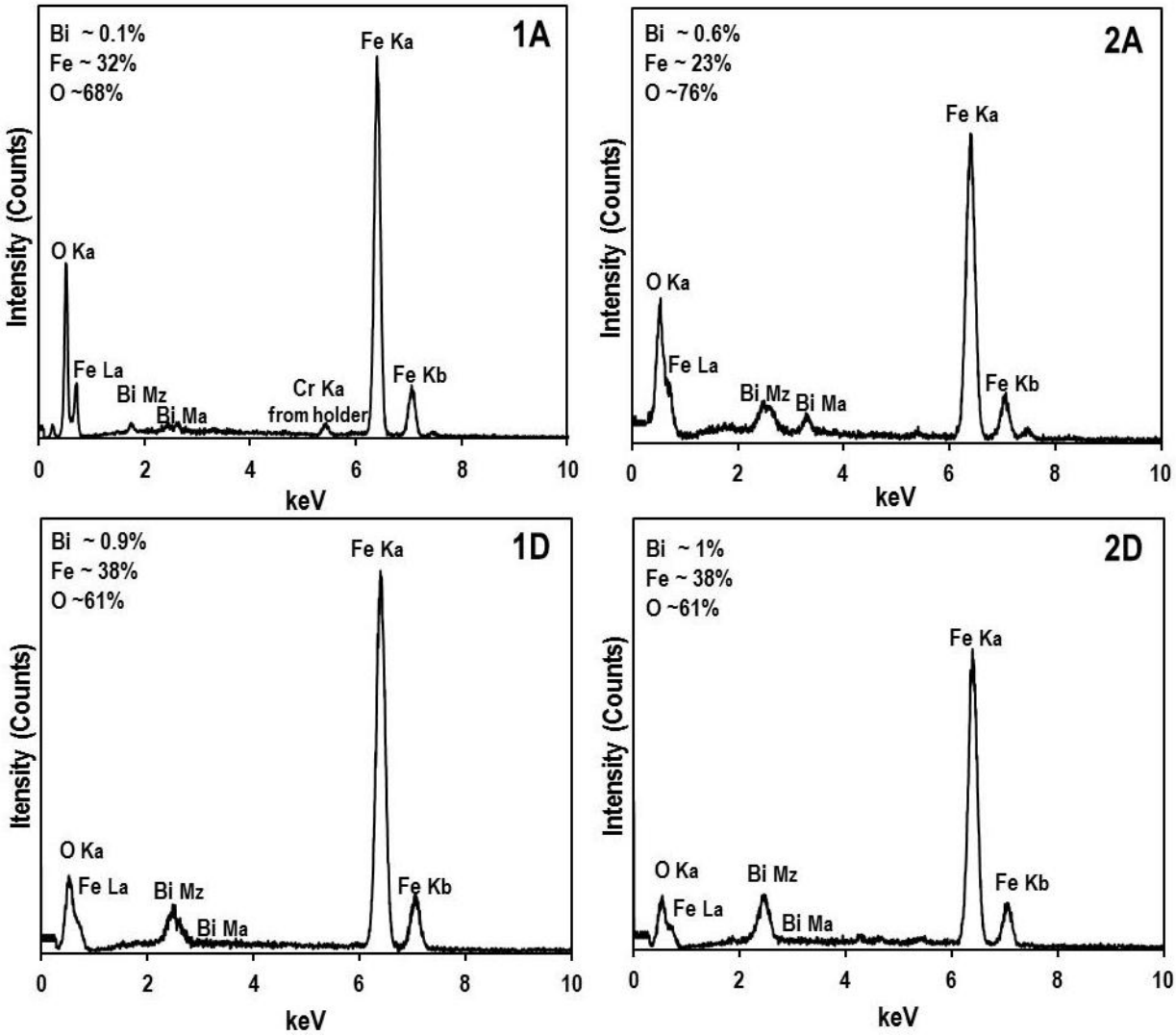

Figure S5. EDS analysis the products washed with acid corresponding to Figure 1A, 2A, 1D and 2D.

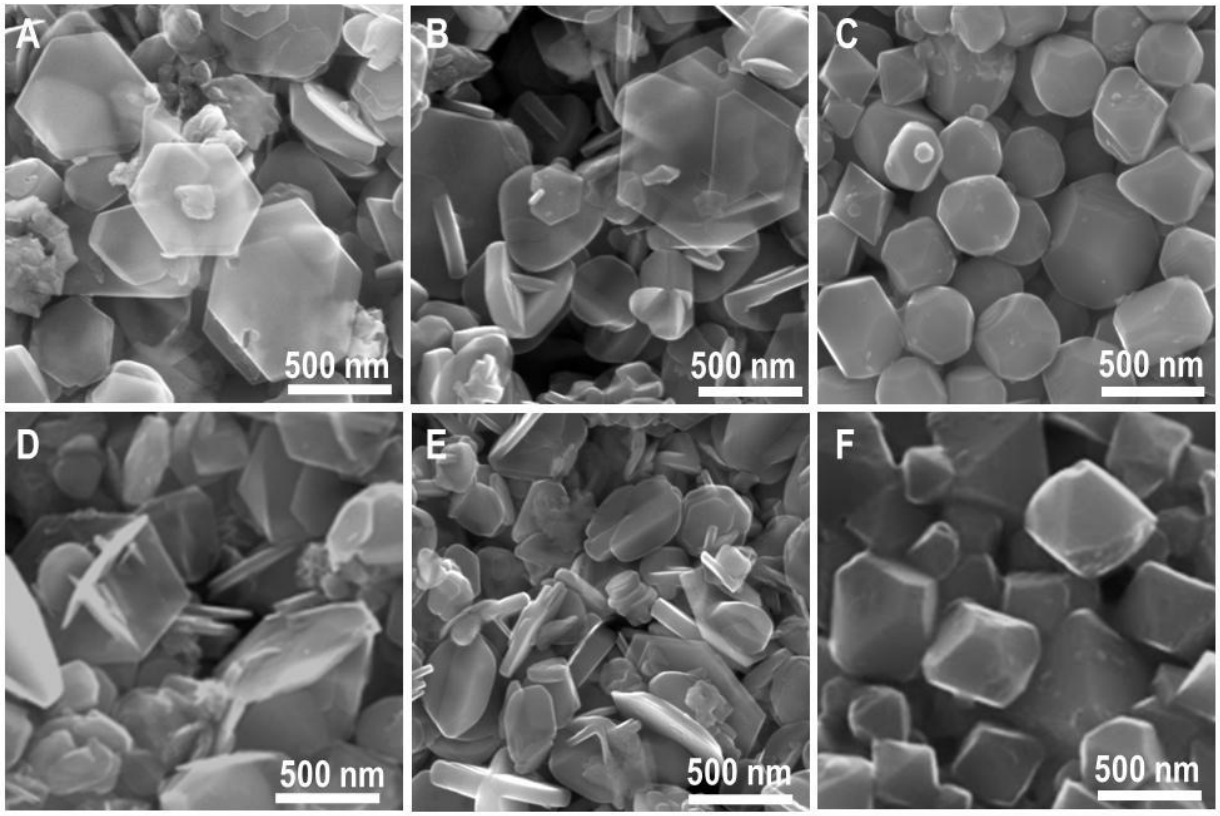

Figure S6. SEM images of the products obtained when (A) α-Fe_2O_3 and Na_2CO_3/$Bi(NO_3)_3$, (B) α-Fe_2O_3 and Rb_2CO_3/$Bi(NO_3)_3$, (C) α-Fe_2O_3 and Li_2CO_3/$Bi(NO_3)_3$, (D) γ-Fe_2O_3 and Na_2CO_3/$Bi(NO_3)_3$, (E) γ-Fe_2O_3 and Rb_2CO_3/$Bi(NO_3)_3$, or (F) γ-Fe_2O_3 and Li_2CO_3/$Bi(NO_3)_3$ are used as the precursor colloid and salt flux, respectively.

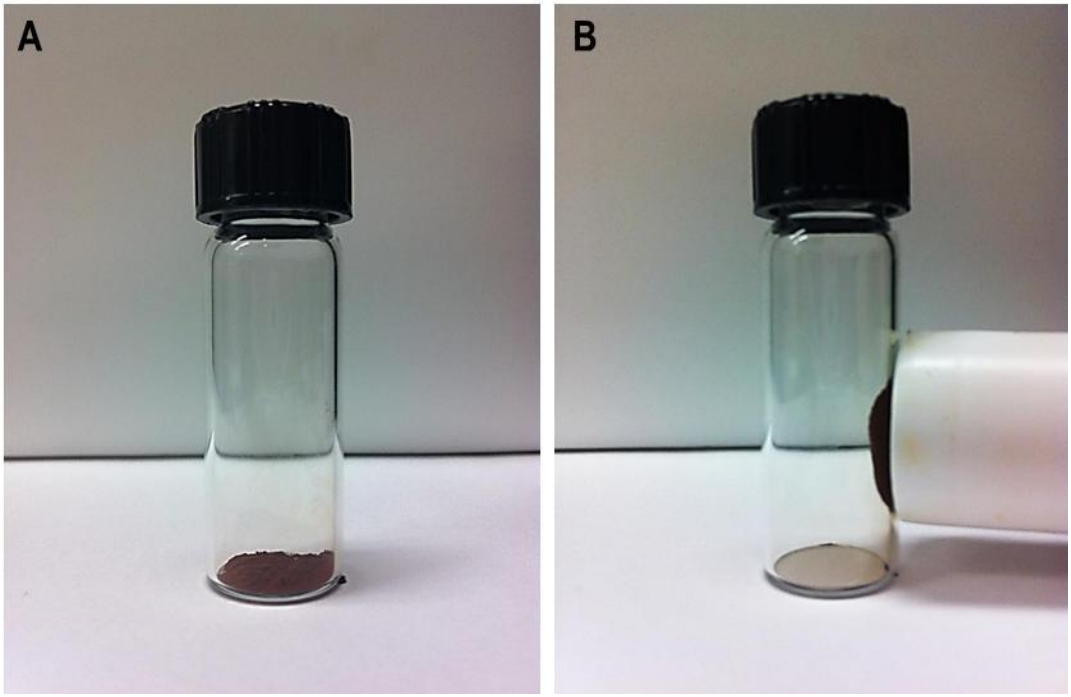

Figure S7. Photographs of the product from the reaction utilizing γ-Fe_2O_3 colloids and $Bi(NO_3)_3/K_2CO_3$ when a magnet (A) is not and (B) is applied.

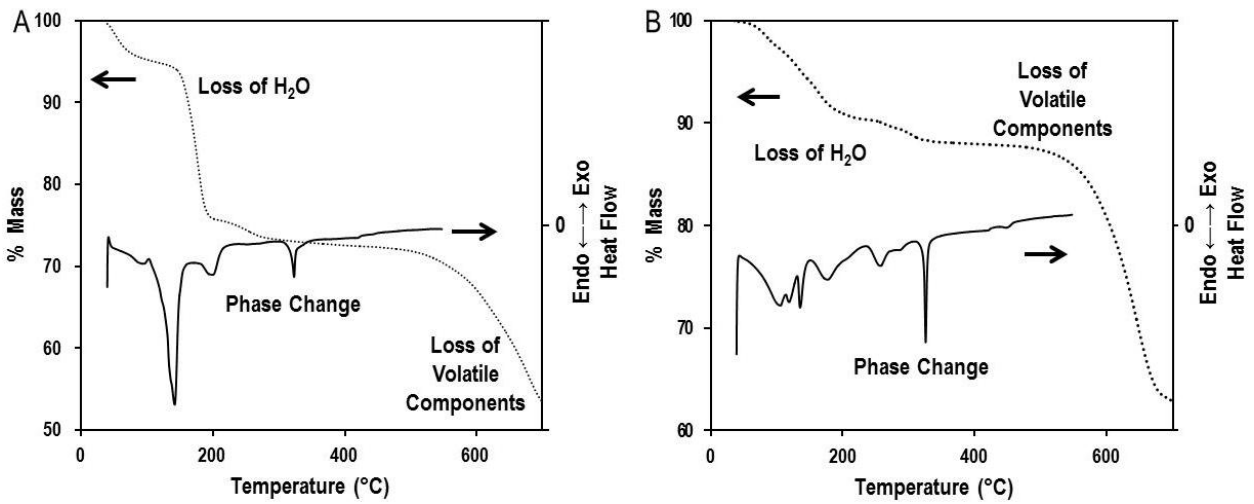

Figure S8. DSC (right axes) and TGA (left axes) of the dried precursors for the reaction utilizing $Bi(NO_3)_3$, K_2CO_3, and (A) α-Fe_2O_3 precursor colloids or (B) γ-Fe_2O_3 precursor colloids.

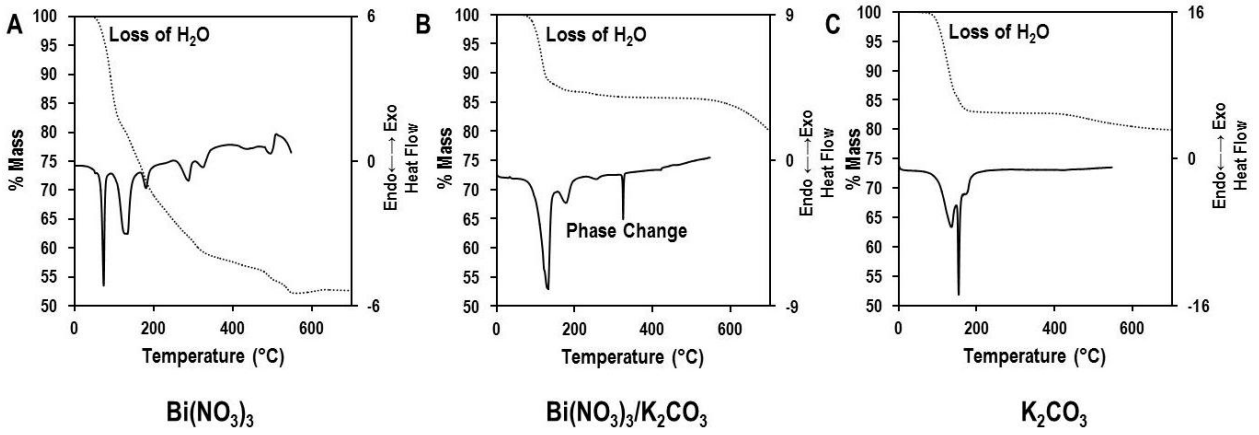

Figure S9. DSC (right axes) and TGA (left axes) of (A) $Bi(NO_3)_3$, (B) $Bi(NO_3)_3$ and K_2CO_3 in a 1:10 ratio, and (C) K_2CO_3 after being dissolved in water then dried under vacuum.

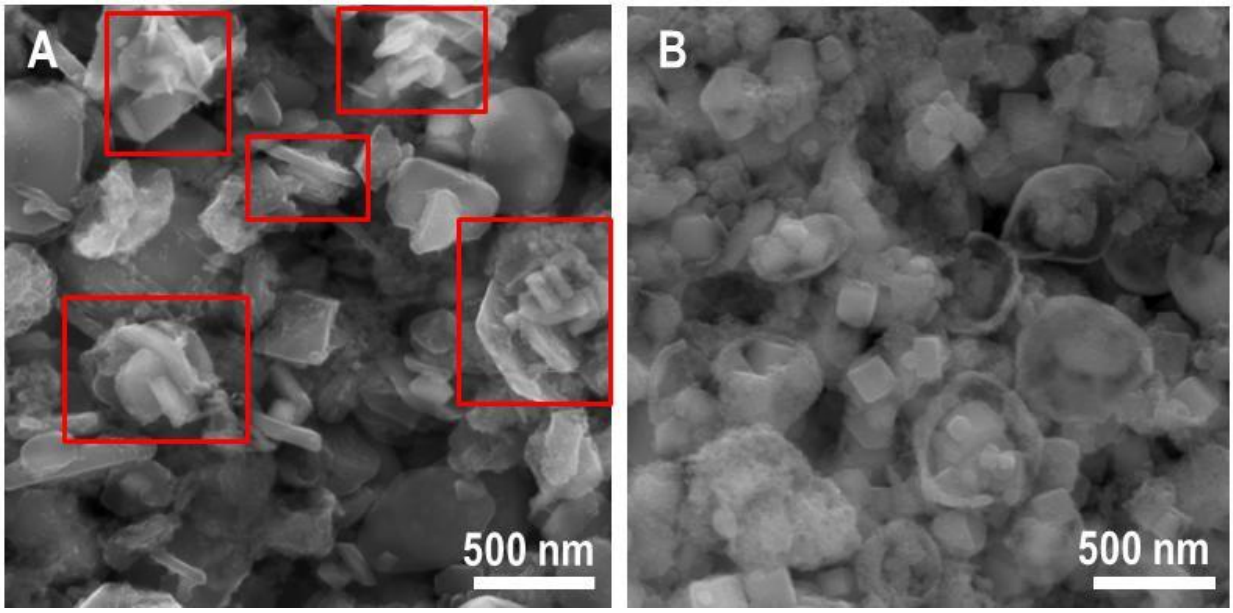

Figure S10. SEM images of flux covered products from the reactions utilizing (A) α-Fe_2O_3 colloids and K_2CO_3/$Bi(NO_3)_3$ (product: α-Fe_2O_3) with areas suggesting multiple plates per droplet highlighted in red boxes and (B) α-Fe_2O_3 colloids and Cs_2CO_3/$Bi(NO_3)_3$ (product: α-Fe_2O_3).